The Journal of Chemical Physics

The effect of temperature on water desalination through two-dimensional nanopores

Cite as: J. Chem. Phys. **152**, 164701 (2020); https://doi.org/10.1063/1.5143069
Submitted: 19 December 2019 . Accepted: 03 April 2020 . Published Online: 23 April 2020

Vishnu Prasad K., and Sarith P. Sathian

The Journal of Chemical Physics ARTICLE scitation.org/journal/jcp

The effect of temperature on water desalination through two-dimensional nanopores

Cite as: J. Chem. Phys. 152, 164701 (2020); doi: 10.1063/1.5143069
Submitted: 19 December 2019 • Accepted: 3 April 2020 •
Published Online: 23 April 2020

Vishnu Prasad K. and Sarith P. Sathian[a)]

AFFILIATIONS

Department of Applied Mechanics, Indian Institute of Technology Madras, Chennai, India

[a)]Author to whom correspondence should be addressed: sarith@iitm.ac.in

ABSTRACT

Two-dimensional (2D) materials such as graphene, molybdenum sulfide, and hexagonal boron nitride are widely studied for separation applications such as water desalination. Desalination across such 2D nanoporous membranes is largely influenced by the bulk transport properties of water, which are, in turn, sensitive to the operating temperature. However, there have been no studies on the effect of temperature on desalination through 2D nanopores. We investigated water desalination through hydrogen functionalized graphene nanopores of varying pore areas at temperatures 275.0 K, 300.0 K, 325.0 K, and 350.0 K. The water flux showed a direct relation with the diffusion coefficient and an inverse relation with the hydrogen-bond lifetime. As a direct consequence, the water flux was found to be related to the temperature as per the Arrhenius equation, similar to an activated process. The results from the present study improve the understanding on water and ion permeation across nanoporous 2D materials at different temperatures. Furthermore, the present investigation suggests a kinetic model, which can predict the water and ion permeation based on the characteristics of the nanopore.

I. INTRODUCTION

Reverse osmosis (RO), a highly efficient membrane-based separation technique, accounts for more than half of the installed desalination capacity across the globe.[1,2] RO also finds applications in food and beverage processing, separation of organic mixtures, and wastewater treatment.[3] In RO, the saline water is forced through a semi-permeable membrane under a pressure gradient to cause retention of ions at the membrane phase.[3] RO possesses immense modern relevance as seawater desalination is looked upon as a solution to the rising global water demand.[2,4] The energy efficiency of RO primarily depends upon the water permeation and the ion exclusion capacity of the membrane.[5] Advanced investigations show a vast scope for improving the state of the art RO systems by introducing novel membrane materials.[6,7]

Nanoporous two-dimensional (2D) materials such as graphene, hexagonal boron nitride (BN), and molybdenum sulfide (MoS_2) show excellent water permeation characteristics as a result of their negligible thickness.[8] Early theoretical studies have demonstrated that nanoporous graphene is very effective as an RO membrane.[9–11] Experimental studies on graphene nanopores have also found water permeation and ion filtration rates in agreement with the theoretical predictions.[12,13] Moreover, a range of studies have been conducted on graphene nanopores of different pore characteristics focusing on water permeation,[14–17] ion selectivity,[18–21] and desalination.[22–29] Furthermore, studies on BN[30–33] and MoS_2[34–36] also show promising results with regard to desalination and molecular separation. Similar investigations are also carried out on other 2D materials such as carbon nitride (C_2N),[37,38] silicon carbide (SiC),[39] graphyne,[40–42] and other derivatives of graphene.[43]

Most above-mentioned studies have only examined the desalination performance at a constant temperature under varying pressure gradients. However, studies on conventional RO membranes have shown that the water and ion permeation rates are sensitive to the operating temperatures.[44,45] For example, studies on carbon nanotube (CNT) membranes by Liu and Patey[46,47] showed that changes in the diffusion coefficient of the water resulting from varying temperatures can grossly influence the flow rates through CNTs. They also found that the flow through CNTs follows the Arrhenius equation, similar to an activated process.[46] A later study by Kurupath *et al.*[48] showed that the water permeation through graphene nanopores depends strongly on the diffusion coefficient of water. Furthermore,

they observed a clear correlation between the flow rates and the hydrogen-bond lifetime of water.[48]

As per the conventional solution-diffusion model of RO,[49] the solute–solvent separation results from a difference in the diffusion coefficient and the membrane phase solubility between the solute (ion) and the solvent (water).[50,51] Hence, an increased operating temperature causes an increased ion osmotic pressure, which, in turn, demands an increased pressure gradient to sustain the permeation.[52] However, in 2D membranes, hydration, electrostatic, and steric mechanisms play a major role in solute–solvent separation.[10] Furthermore, the ion dehydration is found to influence the ion selectivity across 2D nanomembranes.[20,21] This indicates that in 2D membranes, an increased temperature could result in an increased water flux without compromising the ion rejection. Alternatively, a reduced operating temperature can inhibit the ion flux while allowing a significant water flux as observed in CNTs.[47] A recent study along these lines using polyamide (PA) thin-film composite membranes show that with an increase in temperature, the water flux increases, reaches a maximum, and decreases thereafter.[53] However, there have been no investigations so far that report similar results with regard to 2D nanopores.

Here, we investigate water desalination across three hydrogen functionalized nanopores of pore areas 17.6 Å^2, 37.7 Å^2, and 76.3 Å^2 at temperatures 275.0 K, 300.0 K, 325.0 K, and 350.0 K. We consider two methods of heating the system, viz., heating the water and heating the nanoporous membrane. We use non-equilibrium molecular dynamics (NEMD) simulations to calculate the water and the ion flux through the membranes and equilibrium molecular dynamics (EMD) simulations to calculate the bulk transport properties. By comparing the flux with the transport properties obtained at different temperatures, we elucidate a kinetic relationship between the flux and the temperature.

II. METHODOLOGY

Hydrogen functionalized nanopores P1, P2, and P3 of pore areas (A_P) 17.6 Å^2, 37.7 Å^2, and 76.3 Å^2 were created on 30 × 30 Å^2 sized graphene sheets (see Fig. 1 and Fig. S1 of the supplementary material). These nanopores acted as membranes that separated the feed reservoir [60 Å long, containing 1786 water molecules and 17 sodium chloride (NaCl) molecules, corresponding to 0.5 M] from the permeate reservoir (30 Å long, containing 852 water molecules), as shown in Fig. 2. Plane graphene sheets at the ends acted as pistons that pressurized the reservoirs using external force. Additional space was provided beyond the pistons (along the z-axis) to avoid interactions across the boundaries.

The TIP4P/2005 model[54] was used for simulating water, and the ion interactions were modeled using parameters optimized for the TIP4P/2005 model.[55] The intramolecular interactions of the nanopore were modeled using the AIREBO potential.[56,57] The cross-interaction parameters of the carbon atoms and the remaining atoms were calculated using the Lorentz–Berthelot (LB) mixing rule, employing the parameters for carbon from the AMBER force-field.[58,59] The parameters of the functional hydrogen and the associated carbon were taken from the work of Müller-Plathe.[60] The remaining cross-interaction parameters were defined using the LB mixing rules (see Table S1 in the supplementary material). A cut-off of 12 Å was used for the Lennard-Jones (LJ) and the short-range Coulombic interactions, and the Coulombic forces were corrected for long-range effects using the particle–particle–particle–mesh (PPPM) method.[61] The SHAKE algorithm[62] was used to keep the bonds and angles of the water rigid. Periodic boundary conditions (PBC) were applied in all the directions, and a time step of 1 fs was used. All simulations were carried out using the Large-Scale Atomic/Molecular Massively Parallel Simulator (LAMMPS) package.[63]

The energy of the nanoporous membrane was first minimized, keeping the water, ions, and the piston sheets static. The overall energy of the system was then minimized, removing the static constraints. The lateral forces on the piston sheets were neglected, and an axial force that creates 1 atm pressure in both the reservoirs was applied. The system was equilibrated under this condition for 1 ns during which one membrane atom was pinned to its initial position to ensure the positional stability of the membrane. In cases where the water was heated, the feed and permeate reservoirs were kept at the test temperature using the Nosè–Hoover thermostat (NVT),[64] and the membrane temperature was allowed to evolve as per the microcanonical ensemble (NVE). For the cases where the membrane was heated, the feed and permeate reservoirs were kept at 300 K, while the membrane was maintained at the test temperature. During the production run that lasted for 5 ns, the feed side pressure was raised to 200 MPa, keeping the permeate side pressure at the initial value (1 atm). In cases where the membrane was heated, the reservoirs were now decoupled from the thermostat and were merely time integrated. Five random trials were carried out for each nanopore–temperature combination, and the water and the ion permeation across the membrane was recorded every 100 fs.

The diffusion coefficient (D) and the hydrogen-bond lifetime (τ_{hb}) were calculated using equilibrium molecular dynamics (EMD)

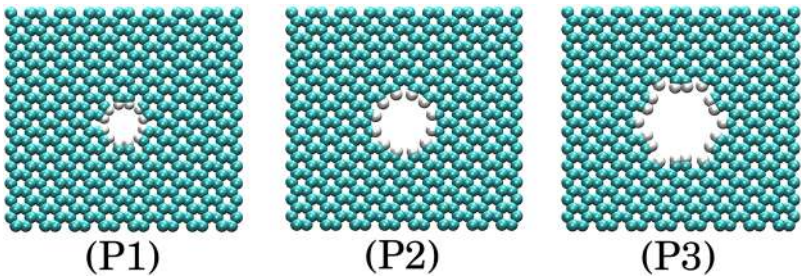

FIG. 1. The nanopores used in this study. Pores P1, P2, and P3 have areas 17.6 Å^2, 37.7 Å^2, and 76.3 Å^2, respectively.

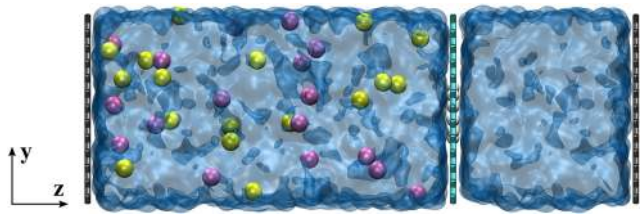

FIG. 2. Snapshot of the system used in this study. The yellow and pink balls represent the sodium (Na^+) and chloride (Cl^-) ions. The cyan sheet in the middle represents the nanopore/membrane. The blue fluid represents the water. The black sheets at the ends represent the piston graphene sheets used for pressurizing the reservoirs.

simulations on a water–ion mixture (1411 water molecules and 13 NaCl molecules, corresponding to 0.5 M). Here, after the initial minimization, the system was equilibrated for 1 ns at 1 atm pressure and the test temperature (NPT). The production run was then carried out for 1 ns at constant volume and temperature (NVT). The atomic trajectories were recorded every femtosecond, and the diffusion coefficient was calculated using the following equation:

$$D = \frac{1}{2N_D\tau(t_L - t_F - \tau)} \sum_{t_0=t_F}^{t_0=t_L-\tau} \frac{1}{N} \sum_{i=1}^{i=N} (r_i(t_0+\tau) - r_i(t_0))^2, \quad (1)$$

where N_D is the number of dimensions (here 3), τ is the time interval, t_F and t_L are the times corresponding to the first and last snapshots of the trajectory, N is the number of water molecules, and $r_i(t)$ is the position vector of the i-th water molecule at time t. The limiting values of the diffusion coefficient at τ = 50 ps, calculated from five 200 ps long sample trajectories, were averaged to obtain the final values.

The hydrogen-bond lifetime (τ_{hb}) was calculated from the hydrogen-bond auto-correlation function [$C(t)$] obtained from the EMD trajectories as per the following equation:[65,66]

$$C(t) = \left\langle \frac{\Sigma h_{ij}(t_0) h_{ij}(t_0+t)}{\Sigma h_{ij}(t_0)^2} \right\rangle_{ij}. \quad (2)$$

Here, $h_{ij}(t_0)$ represents the initial number of hydrogen bonds formed between the donor molecules (represented by the index i) and the acceptor molecules (represented by the index j). $h_{ij}(t_0 + t)$ represents the number of hydrogen bonds that had survived between the initial donor–acceptor (ij) pairs after the time t.[65,66] Ten $C(t)$ vs t curves were averaged, and the following equation [Eq. (3)] was fitted to the resultant so that parameters A_1, τ_1, and τ_2 are obtained,[48]

$$C_{fit}(t) \approx A_1 e^{t/\tau_1} + (1 - A_1) e^{t/\tau_2}. \quad (3)$$

The hydrogen-bond lifetime (τ) is then found by integrating Eq. (3) as follows:[66]

$$\text{Hydrogen-bond lifetime } \tau_{hb} = \int_0^\infty C_{fit}(t). \quad (4)$$

The potential of mean force (PMF) calculations were carried out by coupling EMD simulations with the adaptive biasing forcing (ABF) algorithm.[67] Up to 10 Å preceding, the nanopore was sampled up to 50 ns to ensure the convergence of the results. We have followed the equations and other details of the PMF calculation as reported elsewhere.[48]

III. RESULTS AND DISCUSSION

Figure 3(a) shows the number of water molecules (N_w) crossing the nanopore P2 (A_P = 37.7 Å^2) against time (t) at different temperatures (T). The dotted lines represent the cases where the membrane was heated. Plots for nanopores P1 (A_P = 17.6 Å^2) and P3 (A_P = 76.3 Å^2) are given in Figs. S2 and S3 of the supplementary material. A maximum of 84% difference was observed in the water flux across the nanopore P1 when the temperature was varied from 275.0 K to 350.0 K. In cases where the water was heated, the number of water molecules crossing the membrane varied linearly with time. However, in cases where the membrane was heated, the variation between the number of water molecules crossing the membrane and time (indicative of the flux) was initially non-linear, especially at 350.0 K. This disparity arises from the delayed onset of thermal equilibrium between the water that was maintained at 300.0 K and the membrane that was maintained at 350.0 K until the onset of RO (see Fig. S4 of the supplementary material). After 2 ns of RO, the variation between the number of water molecules crossing the nanopore and time became independent of the heating method. The water flux (Q_w) (defined as the slope between N_w and t) and the ion flux (Q_i) through nanopore P2 are shown in Fig. 3(b). Irrespective of the heating method, an increased temperature caused

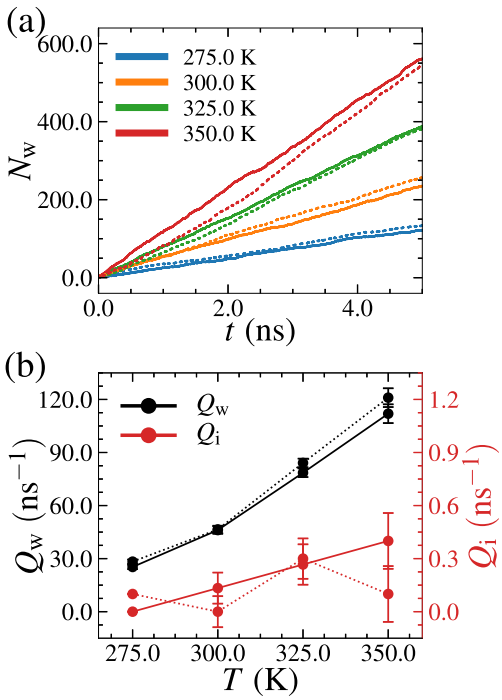

FIG. 3. (a) The number of water molecules crossing the nanopore (N_w) against time (t). (b) The water flux (Q_w) and the ion flux (Q_i) against temperature (T). The data are for nanopore P2 (A_P = 37.7 Å^2). The dotted lines represent the cases where the membrane was heated.

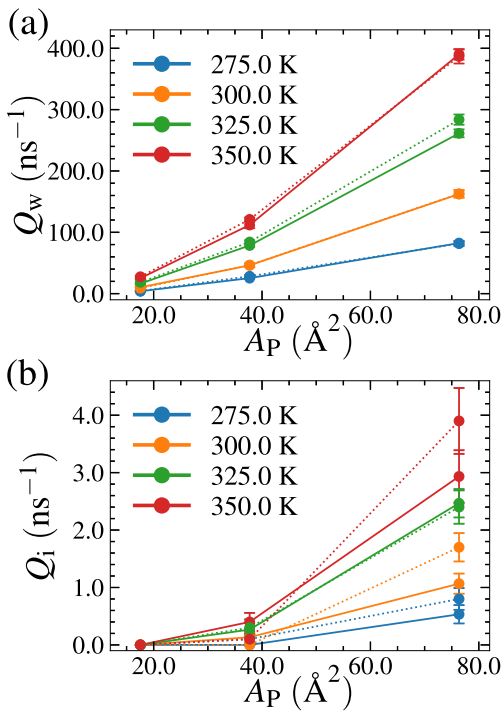

FIG. 4. (a) The water flux (Q_w) and (b) the ion flux (Q_i) against the pore area (A_P) at different temperatures (T). The dotted lines represent the cases where the membrane was heated.

an increased water and ion flux across all the nanomembranes and vice versa. Furthermore, the flux varied minimally between the cases of heating the water and heating the membrane. This indicates that thermally conductive 2D membranes (such as nanoporous graphene[68] or BN[69]) can be heated/cooled to regulate the water/ion permeation.

Figures 4(a) and 4(b) show the water flux (Q_w) and the ion flux (Q_i) against the pore area (A_P) at different temperatures (T). An increase in the pore area resulted in an increased water and ion flux through the membrane, particularly at higher temperatures. There was zero ion permeation through the nanopore P1 (A_P = 17.6 Å^2) at all the temperatures tested. However, higher temperatures resulted in a higher water permeation through P1. This confirms enhancement in water permeation through the membrane with an increase in temperature while retaining the original ion exclusion capacity. In nanopores P2 and P3, a reduced temperature resulted in a reduced ion flux, similar to the case of CNTs.[47] Table I shows the data corresponding to Figs. 4(a) and 4(b). Table S2 and Fig. S5 of the supplementary material provide a comparison between the water flux obtained with previously reported values. The results obtained are in-line with the previous studies.[9,13–15,23,70]

Figure 5(a) shows the variation of water flux through the nanopores (Q_w^{P1}, Q_w^{P2}, and Q_w^{P3}) against the diffusion coefficient (D) obtained from EMD simulations. The dotted lines represent the cases where the membrane was heated. The flux showed a linear relationship with the diffusion coefficient for all the nanopores. The gradient between the flux and the diffusion coefficient was steeper in cases where the pore area was larger. The results are in agreement with the previously observed direct relationship between the water flux and the bulk diffusion coefficient in flow across nanoporous membranes.[46,48] Furthermore, the results are in-line with the previously reported diffusion coefficient values[71–75] (see Table S3 and Fig. S6 of the supplementary material).

Figure 5(b) shows the variation of water flux through the nanopores (Q_w^{P1}, Q_w^{P2}, and Q_w^{P3}) against the hydrogen-bond lifetime of water (τ_{hb}) obtained from the EMD simulations (see Sec. II and Fig. S7 of the supplementary material). Contrary to the case of the diffusion coefficient, the flux showed an inverse relationship with the hydrogen-bond lifetime, i.e., the flux reduced as the

TABLE I. The water flux (Q_w, ns^{-1}) and the ion flux (Q_i, ns^{-1}) through the nanopores (area A_P, Å^2) at different temperatures (T, K). The values in parentheses indicate the standard error.

		Water heated		Membrane heated	
A_P	T	Q_w	Q_i	Q_w	Q_i
17.6 (pore P1)	275.00	3.93(0.41)	0.00 (0.00)	4.30(0.66)	0.00 (0.00)
	300.00	10.33(0.98)	0.00 (0.00)	8.90(1.02)	0.00 (0.00)
	325.00	16.33(1.59)	0.00 (0.00)	18.40(1.88)	0.00 (0.00)
	350.00	25.13(1.28)	0.00 (0.00)	27.50(1.73)	0.00 (0.00)
37.7 (pore P2)	275.00	25.27(1.21)	0.00 (0.00)	28.30(2.27)	0.10 (0.09)
	300.00	46.13(2.10)	0.13 (0.09)	46.50(3.07)	0.00 (0.00)
	325.00	78.53(2.43)	0.27 (0.11)	84.10(2.91)	0.30 (0.14)
	350.00	111.93(5.31)	0.40 (0.16)	121.00(3.15)	0.10 (0.09)
76.3 (pore P3)	275.00	82.40(3.09)	0.53 (0.16)	81.60(4.21)	0.80 (0.19)
	300.00	162.40(5.13)	1.07 (0.18)	162.70(6.30)	1.70 (0.25)
	325.00	261.33(6.49)	2.47 (0.25)	283.70(8.35)	2.40 (0.29)
	350.00	390.07(8.58)	2.93 (0.46)	386.60(11.43)	3.90 (0.57)

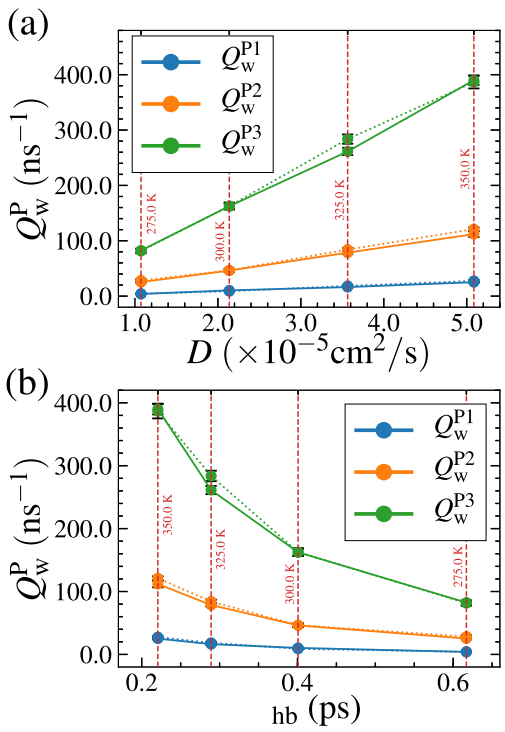

FIG. 5. The variation of water flux through the nanopores (Q_w^{P1}, Q_w^{P2}, and Q_w^{P3}) against (a) the diffusion coefficient (D) and (b) the hydrogen-bond lifetime (τ_{hb}) at different temperatures. The dotted lines represent the cases where the membrane was heated. The diffusion coefficient and the hydrogen-bond lifetime were obtained from the EMD simulations. The red vertical lines are labels to indicate the temperature at each data point.

hydrogen-bond lifetime increased. The results are in agreement with previous studies, where the hydrogen-bond lifetime and the flux were found to show an inverse relationship with each other.[48] Table II shows the values corresponding to Figs. 5(a) and 5(b).

From Fig. 5(a), the water permeation through any nanopore P can be approximated in terms of the diffusion coefficient as follows:

$$Q_w^P = C_1^P + C_2^P (D)^{n_P}, \tag{5}$$

where C_1^P, C_2^P, and n_P are the constants specific to nanopore P. Furthermore, from Fig. 5(b), the water permeation can be written in terms of the hydrogen-bond lifetime as

$$Q_w^P = C_3^P/(\tau_{hb})^{m_P}, \tag{6}$$

where C_3^P and m_P are the constants specific to nanopore P.

To understand the interplay between the bulk transport properties and the flux, the logarithm of the diffusion coefficient [ln(D)] and hydrogen-bond lifetime [ln(τ_{hb})] was plotted against the inverse of temperature ($1/T$), as shown in Fig. 6. The dashed lines represent the fitting curves. The logarithm of the diffusion coefficient showed a linearly decreasing relationship with the inverse of temperature, in conformance with previous studies.[46] On the other hand, the hydrogen-bond lifetime showed a linearly increasing relationship with the inverse of temperature.

The diffusion coefficient–temperature relationship shown in Fig. 6 can be approximated using an Arrhenius formulation as follows:[46,73]

$$\ln(D) = C_4' - \frac{C_5}{T}. \tag{7}$$

Assuming that $C_4' = \ln(C_4)$, the above equation can be rewritten as

$$D = C_4 e^{(-C_5/T)}, \tag{8}$$

where, C_4', C_4, and C_5 are the constants. It should be noted that when the temperature range lies largely below 290 K, the Speedy–Angel (SA) or the Vogel–Fulcher–Tamann (VFT) formulations should be used to describe the diffusivity–temperature relation.[76] However, in the present study, the diffusivity–temperature relation can be assumed to follow Eq. (8) since the percentage average absolute deviation [%AAD; see Eq. (1) of the supplementary material for details][76] between the fitted curve and the original data is less than 5%. From Fig. 6, the hydrogen-bond lifetime and the temperature can also be related as

$$\ln(\tau_{hb}) = C_6' + \frac{C_7}{T}. \tag{9}$$

Assuming that $C_6' = \ln(C_6)$, the above equation can also be rewritten as

TABLE II. The water flux through the nanopores (Q_w^{P1}, Q_w^{P2}, and Q_w^{P3}, ns^{-1}), the diffusion coefficient (D, $\times$ 10^{-5} cm^2 s^{-1}), and the hydrogen-bond lifetime (τ_{hb}, ps) at different temperatures (T, K). The values in parentheses indicate the standard error.

T	Q_w^{P1}	Q_w^{P2}	Q_w^{P3}	D	τ_{hb}
275.00	3.93(0.41)	25.27(1.21)	82.40(3.09)	1.07	0.62
300.00	10.33(0.98)	46.13(2.10)	162.40(5.13)	2.14	0.40
325.00	16.33(1.59)	78.53(2.43)	261.33(6.49)	3.56	0.29
350.00	25.13(1.28)	111.93(5.31)	390.07(8.58)	5.09	0.22

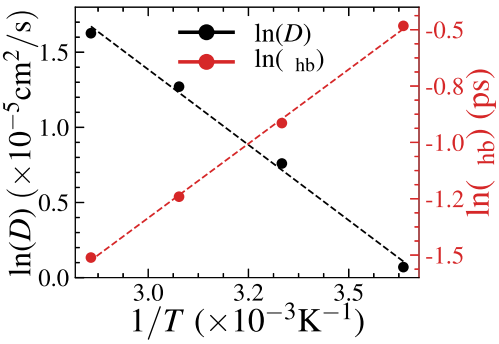

FIG. 6. Logarithmic variation of the diffusion coefficient (D) and the hydrogen-bond lifetime (τ_{hb}) against the inverse of temperature ($1/T$). The dashed lines represent the fitting curves. The diffusion coefficient and the hydrogen-bond lifetime were obtained from the EMD simulations.

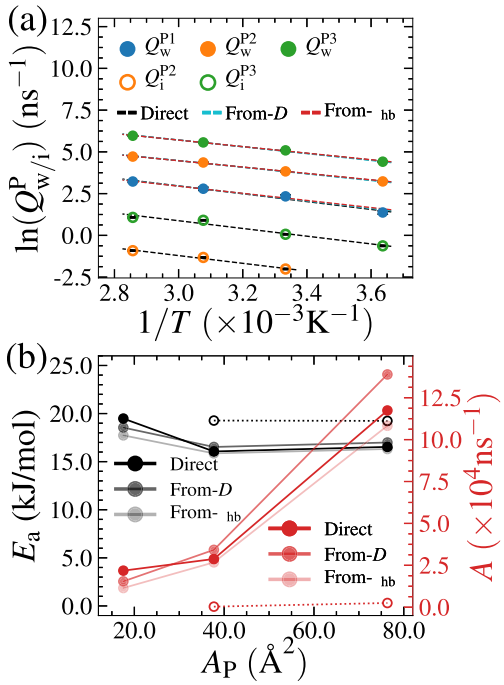

FIG. 7. (a) The logarithmic variation of water flux (Q_w) and ion flux (Q_i) through the nanopores (P1, P2, and P3) against the inverse of temperature ($1/T$). The dashed lines represent the fitting curves obtained using different methods. (b) The variation of Arrhenius activation energy (E_a) and the pre-exponential factor (A) against the pore area (A_P). The color intensities represent the data obtained using different fitting methods. The dotted lines represent the data corresponding to ion permeation.

$$\tau_{hb} = C_6 e^{(C_7/T)}, \tag{10}$$

where C_6', C_6, and C_7 are the constants.

From Eq. (5), $C_1^P = 0$ (since $D = 0$ implies that $Q_w^P = 0$). Hence, combining Eqs. (5) and (8), we get

$$Q_w^P = C_2^P (C_4)^{n_P} e^{(-n_P C_5/T)}. \tag{11}$$

Similarly, combining Eqs. (6) and (10), we get

$$Q_w^P = \frac{C_3^P}{(C_6)^{m_P}} e^{(-m_P C_7/T)}. \tag{12}$$

Both Eqs. (11) and (12) can be rewritten as an Arrhenius-like equation as follows:

$$Q_w^P = k_1^P e^{(-k_2^P/T)}. \tag{13}$$

Here, k_1^P is equal to $C_2^P (C_4)^{n_P}$ or $\frac{C_3^P}{(C_6)^{m_P}}$ and k_2^P is equal to $n_P C_5$ or $m_P C_7$. Furthermore, taking logarithm on both sides, Eq. (13) can be modified as

$$\ln(Q_w^P) = \ln(A) - \frac{E_a}{RT}, \tag{14}$$

where A is the pre-exponential factor, which is equal to k_1^P, E_a is the Arrhenius activation energy, which is equal to $k_2^P R$, and R is the universal gas constant. This indicates that the flow through 2D nanopores behaves like an activated process, similar to the flow through CNTs.[9,46,77]

To understand the activated behavior of water flow through the nanopores, the logarithm of the water/ion flux [$\ln(Q_{w/i}^P)$] was plotted against the inverse of temperature ($1/T$), as shown in Fig. 7(a). The dashed lines represent the fitting curves that were obtained using three different methods, namely, Direct, From-D, and From-τ_{hb}. The fitting curves labeled Direct were obtained by fitting the flux and temperature data directly to Eq. (13). For obtaining the fitting curves labeled From-D, first, the parameters C_2^P and n_P from Eq. (5) (see Fig. S9 of the supplementary material) and C_4^P and C_5^P from Eq. (8) were found. These parameters were then used to find k_1^P and k_2^P as per Eq. (13), and the curves were obtained. A similar procedure is used for the curves labeled From-τ_{hb}, except that the parameters C_3^P, m_P (see Fig. S8 of the supplementary material), C_6, and C_7 from Eqs. (6) and (10) were used to determine k_1^P and k_2^P. Table III provides the fitting parameters obtained from different methods. The Direct method alone was used to find the fitting curves for ion permeation data.

Except for nanopore P1, the fitting curves obtained using different methods showed minimal variation among each other. However, the parameter k_1^P (equal to the pre-exponential factor, A) obtained using different fitting methods showed variation to some extent. This has occurred due to the cumulation of fitting errors in From-D and From-τ_{hb} methods since two stages of fitting are done in these methods to obtain the final curve. Table IV provides the %AAD of the different fitting curves for the temperature–flux variation [given in Fig. 7(a)].

TABLE III. The fitting parameters obtained using different methods. k_1^P is expressed in $\times 10^4$ ns^{-1}, and k_2^P is expressed in $\times 10^3$ K. C_2^P is expressed in $(\times 10^{-5}\text{cm}^2/\text{s})^{n_P}\text{ns}^{-1}$, and C_3^P is expressed in $(\text{ps})^{m_P}\text{ns}^{-1}$. n_P and m_P have arbitrary units. The fitting parameters obtained from Eqs. (8) and (10) are as follows: $C_4 = 1649.60 \times 10^{-5}$ cm^2/s, $C_5 = 2.01 \times 10^3$ K, $C_6 = 5.05 \times 10^{-3}$ ps, and $C_7 = 1.32 \times 10^3$ K.

	Direct			From-D				From-τ_{hb}		
Pore	k_1^P	k_2^P	C_2^P	n_P	k_1^P	k_2^P	C_3^P	m_P	k_1^P	k_2^P
P1	2.18	2.34	4.10	1.11	1.54	2.23	2.19	1.62	1.14	2.13
P2	2.88	1.93	22.32	0.99	3.42	1.99	12.66	1.45	2.67	1.91
P3	11.74	1.99	73.79	1.02	13.89	2.04	41.17	1.49	10.83	1.96

TABLE IV. The %AAD obtained between the fitted curves and the data points of temperature–flux variation [Fig. 7(a)] using different fitting methods.

Method\Nanopore	P1	P2	P3
Direct	4.16	0.51	0.55
From-D	4.81	0.70	0.50
From-τ_{hb}	5.37	0.60	0.58

The Direct method showed the least %AAD among all the methods. However, for nanopore P3, the %AAD obtained using the from-D method was slightly lower than the Direct method. The %AAD was found to be higher for nanopore P1 when compared to nanopores P2 and P3. This is because water permeation through P1 at lower temperatures (300.0 K and 275.0 K) deviates from the Arrhenius formulation [see Fig. 7(a)]. However, since the water flux through such a small nanopore at lower temperatures is highly inconsistent, a more extensive study is needed to establish this understanding.[77] Nevertheless, the parameters obtained using the Direct method can be used to characterize desalination through the nanopores as their maximum %AAD is below 5%.

Across the nanopores, the fitting curves showed similar slopes, indicating a minimal variation in Arrhenius activation energy among the pores [Fig. 7(a)]. However, the intercepts of the curves that are indicative of the pre-exponential factor varied widely among the nanopores. Similar trends were also observed for the ion flux. Ion permeation events did not occur for nanopore P1, and for pore P2, they occurred below 300 K (see Table I), and hence, the data are not shown in this figure.

Figure 7(b) shows the Arrhenius activation energy (E_a) and the pre-exponential factor (A) obtained using different fitting methods against the area of the nanopores (A_P). In all the cases, the activation energy of nanopores was similar except for pore P1, which had slightly larger activation energy compared to pores P2 and P3. On the other hand, the pre-exponential factor (A) obtained increased monotonously with the pore area, showing large variation between the pores P1 and P3 compared to the difference between pores P1 and P2. As mentioned earlier, the pre-exponential factors (the same as k_1^P) obtained using different fitting methods varied to some extent due to the difference in how the parameters are derived in each method. Table S4 of the supplementary material shows the data corresponding to Fig. 7(b).

The Arrhenius activation energy is indicative of the barrier that water molecules have to overcome to cross the nanopore. Hence, it is expected that the Arrhenius activation energy and the free energy barrier calculated from PMF profiles would follow a similar trend with varying pore area (see Fig. 8). As per the classical Arrhenius formulation, the pre-exponential factor is defined as the frequency of molecular collisions with the required energy and orientation during a reaction.[78] In the case of nanoporous membranes, this may be assumed as the attempt rate of molecules to cross the nanopore.[9] We infer the pre-exponential factor to be primarily dependent on the pore occupancy, the structure of water inside the nanopore, and the energy of the water/ion molecules. However, the quantification of the pre-exponential factor requires a further study.

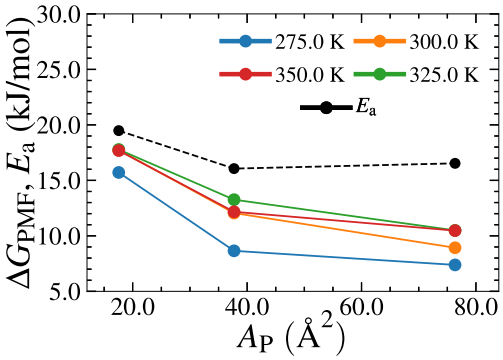

FIG. 8. The free energy barrier obtained from PMF calculations (ΔG_{PMF}) against the pore area (A_P) at various temperatures. The black dashed line represents the Arrhenius activation energy (E_a) obtained using the Direct method.

Figure 8 shows the free energy barrier experienced by the water (ΔG_{PMF}) against the pore area (A_P) at different temperatures (T). The free energy barrier was found by subtracting the minimum energy from the maximum energy of the PMF profile ahead of the nanopore (see Fig. S9 of the supplementary material). The black dashed line represents the Arrhenius activation energy (E_a) obtained using the Direct method. The variation of the free energy barrier was similar across the temperatures considered. The Arrhenius activation energy also showed a similar trend though their values were higher than the free energy barriers obtained from the PMF calculations. The Arrhenius activation energy and the pre-exponential factor can be related to the Gibbs activation energy ($\Delta G^{\neq}$) as per the transition state theory (TST).[79] The Gibbs activation energy ($\Delta G^{\neq}$), in turn, can be related to the PMF energy barrier (ΔG_{PMF}).[80] However, the application of TST to establish a relationship between the empirically derived Arrhenius parameters and the PMF energy barrier requires more extensive studies. Meanwhile, the Arrhenius framework may be utilized in experimental methods for quantifying performance scale-up.[77,81,82]

IV. CONCLUSIONS

We studied the effect of temperature on water desalination through hydrogen functionalized graphene nanopores. We used three nanopores of areas 17.6, 37.7, and 76.3 Å^2 and the temperatures 275.0 K, 300.0 K, 325.0 K, and 350.0 K in this study. Furthermore, for each nanopore–temperature combination, the calculations were carried out using two distinct heating methods, viz., heating the water and heating the nanoporous membrane. Among the nanopores that we studied, a maximum of 84% difference in flux was observed across the nanopore P1 when the temperature was varied from 275.0 K to 350.0 K. There was minimal difference in the flux between the cases where the water was heated and the membrane was heated. Furthermore, the flux was found to be related directly with the diffusion coefficient and inversely with the hydrogen-bond lifetime. Our results suggest an Arrhenius-like relationship between the flux and the operating temperature by which the flux through a nanopore can be defined in terms of the activation energy across the pore and a pre-exponential factor. The activation energies obtained

from the Arrhenius formulation were found to be higher than the free energy barriers estimated from the PMF profiles.

Our results indicate that the operating temperatures largely influence the desalination characteristics of 2D nanoporous membranes. Furthermore, the results provide insights for designing water desalination systems employing 2D nanoporous membranes when the operating temperatures vary significantly. The results also show that thermally conducting 2D membranes such as graphene or BN can be heated or cooled to achieve the requisite water/ion permeation characteristics. At higher temperatures, water permeation through smaller nanopores can be improved while maintaining the ion exclusion capacity. On the other hand, a lower temperature can impede ion permeation through larger nanopores at the cost of reduced water permeation. Our results also point to a kinetic relation between the flux and the operating temperature, which can aid in scaling-up the performance parameters of water desalination through 2D membranes.

SUPPLEMENTARY MATERIAL

See the supplementary material for the details of pore area calculation and the interaction parameters used. Water and ion permeation through nanopores P1 and P3 are given. The variation of feed temperature with time for the case where the membrane was heated at 350 K is also given. Furthermore, the water flux and diffusion coefficients from the present study are compared with previous studies. Details of the hydrogen-bond lifetime calculations, the %AAD calculations, the curve fitting methods used, and the PMF energy barrier calculations are provided. Finally, the Arrhenius activation energies and the pre-exponential factors obtained for the nanopores are tabulated.

ACKNOWLEDGMENTS

The authors would like to thank the financial support received from the Department of Science and Technology (DST), Government of India, under Water Technology Initiative [Project No. DST/TM/WTI/2K15/84(G)]. The authors also acknowledge the P. G. Senapathy Center for Computing Resources at IIT Madras for providing access to the VIRGO supercluster.

REFERENCES

[1] S. Miller, H. Shemer, and R. Semiat, Desalination **366**, 2 (2015).
[2] M. Elimelech and W. A. Phillip, Science **333**, 712 (2011).
[3] I. G. Wenten and K. Khoiruddin, Desalination **391**, 112 (2016).
[4] R. F. Service, Science **313**, 1088 (2006).
[5] J. R. Werber, A. Deshmukh, and M. Elimelech, Environ. Sci. Technol. Lett. **3**, 112 (2016).
[6] F. Zhou, M. Fathizadeh, and M. Yu, Annu. Rev. Chem. Biomol. Eng. **9**, 17 (2018).
[7] D. Cohen-Tanugi and J. C. Grossman, Desalination **366**, 59 (2015).
[8] Z. Zheng, R. Grünker, and X. Feng, Adv. Mater. **28**, 6529 (2016).
[9] D. Cohen-Tanugi and J. C. Grossman, Nano Lett. **12**, 3602 (2012).
[10] D. Konatham, J. Yu, T. A. Ho, and A. Striolo, Langmuir **29**, 11884 (2013).
[11] D. Cohen-Tanugi and J. C. Grossman, J. Chem. Phys. **141**, 074704 (2014).
[12] S. C. O'Hern, M. S. H. Boutilier, J.-C. Idrobo, Y. Song, J. Kong, T. Laoui, M. Atieh, and R. Karnik, Nano Lett. **14**, 1234 (2014).
[13] S. P. Surwade, S. N. Smirnov, I. V. Vlassiouk, R. R. Unocic, G. M. Veith, S. Dai, and S. M. Mahurin, Nat. Nanotechnol. **10**, 459 (2015).
[14] M. E. Suk and N. R. Aluru, J. Phys. Chem. Lett. **1**, 1590 (2010).
[15] M. E. Suk and N. R. Aluru, RSC Adv. **3**, 9365 (2013).
[16] C. Zhu, H. Li, and S. Meng, J. Chem. Phys. **141**, 18C528 (2014).
[17] L. Garnier, A. Szymczyk, P. Malfreyt, and A. Ghoufi, J. Phys. Chem. Lett. **7**, 3371 (2016).
[18] K. Sint, B. Wang, and P. Král, J. Am. Chem. Soc. **130**, 16448 (2008).
[19] M. E. Suk and N. R. Aluru, J. Chem. Phys. **140**, 084707 (2014).
[20] S. Sahu, M. Di Ventra, and M. Zwolak, Nano Lett. **17**, 4719 (2017).
[21] S. Sahu and M. Zwolak, Nanoscale **9**, 11424 (2017).
[22] Q. Chen and X. Yang, J. Membr. Sci. **496**, 108 (2015).
[23] Y. Wang, Z. He, K. M. Gupta, Q. Shi, and R. Lu, Carbon **116**, 120 (2017).
[24] R. Guerrero-Avilés and W. Orellana, Phys. Chem. Chem. Phys. **19**, 20551 (2017).
[25] M. Shahbabaei, D. Tang, and D. Kim, Comput. Mater. Sci. **128**, 87 (2017).
[26] R. Jafarzadeh, J. Azamat, and H. Erfan-Niya, Struct. Chem. **29**, 1845 (2018).
[27] Z. Zhang, F. Zhang, Z. Liu, G. Cheng, X. Wang, and J. Ding, Nanomaterials **8**, 805 (2018).
[28] Y. Chen, Y. Zhu, Y. Ruan, N. Zhao, W. Liu, W. Zhuang, and X. Lu, Carbon **144**, 32 (2019).
[29] C. T. Nguyen and A. Beskok, Phys. Chem. Chem. Phys. **21**, 9483 (2019).
[30] H. Gao, Q. Shi, D. Rao, Y. Zhang, J. Su, Y. Liu, Y. Wang, K. Deng, and R. Lu, J. Phys. Chem. C **121**, 22105 (2017).
[31] G. C. Loh, Nanotechnology **30**, 055401 (2018).
[32] X. Davoy, A. Gellé, J.-C. Lebreton, H. Tabuteau, A. Soldera, A. Szymczyk, and A. Ghoufi, ACS Omega **3**, 6305 (2018).
[33] C. Chen, S. Qin, D. Liu, J. Wang, G. Yang, Y. Su, L. Zhang, W. Cao, M. Ma, Y. Qian, Y. Liu, J. Z. Liu, and W. Lei, ACS Appl. Mater. Interfaces **11**, 30430 (2019).
[34] M. Heiranian, A. B. Farimani, and N. R. Aluru, Nat. Commun. **6**, 8616 (2015).
[35] W. Li, Y. Yang, J. K. Weber, G. Zhang, and R. Zhou, ACS Nano **10**, 1829 (2016).
[36] H. Li, T.-J. Ko, M. Lee, H.-S. Chung, S. S. Han, K. H. Oh, A. Sadmani, H. Kang, and Y. Jung, Nano Lett. **19**, 5194 (2019).
[37] Y. Yang, W. Li, H. Zhou, X. Zhang, and M. Zhao, Sci. Rep. **6**, 29218 (2016).
[38] M. Fakhraee and O. Akhavan, J. Phys. Chem. B **123**, 8740 (2019).
[39] R. Jafarzadeh, J. Azamat, and H. Erfan-Niya, Struct. Chem. **31**, 293 (2019).
[40] J. Kou, X. Zhou, H. Lu, F. Wu, and J. Fan, Nanoscale **6**, 1865 (2014).
[41] M. Akhavan, J. Schofield, and S. Jalili, Phys. Chem. Chem. Phys. **20**, 13607 (2018).
[42] M. Raju, P. B. Govindaraju, A. C. T. van Duin, and M. Ihme, Nanoscale **10**, 3969 (2018).
[43] Y. G. Yan, W. S. Wang, W. Li, K. P. Loh, and J. Zhang, Nanoscale **9**, 18951 (2017).
[44] M. F. A. Goosen, S. S. Sablani, S. S. Al-Maskari, R. H. Al-Belushi, and M. Wilf, Desalination **144**, 367 (2002).
[45] W. J. Lau, A. F. Ismail, N. Misdan, and M. A. Kassim, Desalination **287**, 190 (2012).
[46] L. Liu and G. N. Patey, J. Chem. Phys. **144**, 184502 (2016).
[47] L. Liu and G. N. Patey, J. Chem. Phys. **146**, 074502 (2017).
[48] V. P. Kurupath, S. K. Kannam, R. Hartkamp, and S. P. Sathian, Phys. Chem. Chem. Phys. **20**, 16005 (2018).
[49] C. H. Lee, J. Appl. Polym. Sci. **19**, 83 (1975).
[50] D. Paul, J. Membr. Sci. **241**, 371 (2004).
[51] J. Wang, D. S. Dlamini, A. K. Mishra, M. T. M. Pendergast, M. C. Y. Wong, B. B. Mamba, V. Freger, A. R. D. Verliefde, and E. M. V. Hoek, J. Membr. Sci. **454**, 516 (2014).
[52] Y. M. Kim, S. J. Kim, Y. S. Kim, S. Lee, I. S. Kim, and J. H. Kim, Desalination **238**, 312 (2009).
[53] K. Li, L. Liu, H. Wu, S. Li, C. Yu, Y. Zhou, W. Huang, and D. Yan, Phys. Chem. Chem. Phys. **20**, 29996 (2018).

[54]J. L. F. Abascal and C. Vega, J. Chem. Phys. **123**, 234505 (2005).
[55]A. L. Benavides, M. A. Portillo, V. C. Chamorro, J. R. Espinosa, J. L. F. Abascal, and C. Vega, J. Chem. Phys. **147**, 104501 (2017).
[56]S. J. Stuart, A. B. Tutein, and J. A. Harrison, J. Chem. Phys. **112**, 6472 (2000).
[57]D. W. Brenner, O. A. Shenderova, J. A. Harrison, S. J. Stuart, B. Ni, and S. B. Sinnott, J. Phys.: Condens. Matter **14**, 783 (2002).
[58]W. D. Cornell, P. Cieplak, C. I. Bayly, I. R. Gould, K. M. Merz, D. M. Ferguson, D. C. Spellmeyer, T. Fox, J. W. Caldwell, and P. A. Kollman, J. Am. Chem. Soc. **118**, 2309 (1996).
[59]T. A. Beu, J. Chem. Phys. **132**, 164513 (2010).
[60]F. Müller-Plathe, Macromolecules **29**, 4782 (1996).
[61]R. W. Hockney and J. W. Eastwood, *Computer Simulation Using Particles* (CRC Press, 1988).
[62]J.-P. Ryckaert, G. Ciccotti, and H. J. C. Berendsen, J. Comput. Phys. **23**, 327 (1977).
[63]S. Plimpton, J. Comput. Phys. **117**, 1 (1995).
[64]D. J. Evans and B. L. Holian, J. Chem. Phys. **83**, 4069 (1985).
[65]D. C. Rapaport, Mol. Phys. **50**, 1151 (1983).
[66]R. J. Gowers and P. Carbone, J. Chem. Phys. **142**, 224907 (2015).
[67]J. Comer, J. C. Gumbart, J. Hénin, T. Lelièvre, A. Pohorille, and C. Chipot, J. Phys. Chem. B **119**, 1129 (2015).
[68]A. A. Balandin, S. Ghosh, W. Bao, I. Calizo, D. Teweldebrhan, F. Miao, and C. N. Lau, Nano Lett. **8**, 902 (2008).
[69]Q. Cai, D. Scullion, W. Gan, A. Falin, S. Zhang, K. Watanabe, T. Taniguchi, Y. Chen, E. J. G. Santos, and L. H. Li, Sci. Adv. **5**, eaav0129 (2019).
[70]S. C. O'Hern, D. Jang, S. Bose, J.-C. Idrobo, Y. Song, T. Laoui, J. Kong, and R. Karnik, Nano Lett. **15**, 3254 (2015).
[71]M. Holz, S. R. Heil, and A. Sacco, Phys. Chem. Chem. Phys. **2**, 4740 (2000).
[72]R. Mills, J. Phys. Chem. **77**, 685 (1973).
[73]C. Vega, J. L. F. Abascal, M. M. Conde, and J. L. Aragones, Faraday Discuss. **141**, 251 (2009).
[74]O. A. Moultos, I. N. Tsimpanogiannis, A. Z. Panagiotopoulos, and I. G. Economou, J. Phys. Chem. B **118**, 5532 (2014).
[75]R. Fuentes-Azcatl and J. Alejandre, J. Phys. Chem. B **118**, 1263 (2014).
[76]I. N. Tsimpanogiannis, O. A. Moultos, L. F. M. Franco, M. B. d. M. Spera, M. Erdős, and I. G. Economou, Mol. Simul. **45**, 425 (2018).
[77]H. Malmir, R. Epsztein, M. Elimelech, and A. Haji-Akbari, Matter **2**, 735 (2020).
[78]M. Menzinger and R. Wolfgang, Angew. Chem., Int. Ed. **8**, 438 (1969).
[79]J. H. Espenson, *Chemical Kinetics and Reaction Mechanisms* (McGraw-Hill New York, 1995), Vol. 102.
[80]G. K. Schenter, B. C. Garrett, and D. G. Truhlar, J. Chem. Phys. **119**, 5828 (2003).
[81]M. Kumar, M. Grzelakowski, J. Zilles, M. Clark, and W. Meier, Proc. Natl. Acad. Sci. U. S. A. **104**, 20719 (2007).
[82]L. A. Richards, B. S. Richards, B. Corry, and A. I. Schäfer, Environ. Sci. Technol. **47**, 1968 (2013).